# High Refractive Index Hyperbranched Polyvinylsulfides for Planar One-Dimensional All-Polymer Photonic Crystals

Serena Gazzo,[1] Giovanni Manfredi,[1] Robert Pötzsch,[2] Qiang Wei,[2,3] Marina Alloisio,[1] Brigitte Voit,[2,3] Davide Comoretto[1]

[1]Dipartimento di Chimica e Chimica Industriale, Università Di Genova, via Dodecaneso 31, Genova 16146, Italy
[2]Leibniz-Institut für Polymerforschung Dresden E.V., Hohe Straße 6, Dresden 01069, Germany
[3]Center for Advancing Electronics Dresden (Cfaed), Technische Universität Dresden, 01062, Germany
Correspondence to: D. Comoretto (E-mail: davide.comoretto@unige.it)

**ABSTRACT**: We report on the growth and characterization of one-dimensional (1D) planar all-polymer photonic crystals (PhC) with high dielectric contrast ($\Delta n = 0.3$) prepared by spin coating using hyperbranched polyvinylsulfide polymers (HB-PVS) as high refractive index material and cellulose acetate as low refractive index material. Solution processable HB-PVS show a near ultraviolet absorption inducing an increased refractive index in the visible-near infrared ($n = 1.68$, $\lambda = 1000$ nm). HBPVS:Cellulose Acetate Distributed Bragg Reflectors show a very clear fingerprint of the photonic band gap possessing the expected polarized dispersion properties as a function of the incidence angle.

Moreover, engineered microcavities tuned on the weak fluorescence spectrum of the HB-PVS show directional fluorescence enhancement effects due to spectral redistribution of the emission oscillator strength. The combination of all these properties testifies the high optical quality of the obtained photonic structures thus indicating HB-PVS as an interesting material for the preparation of such PhC. © 2015 Wiley Periodicals, Inc. J. Polym. Sci., Part B: Polym. Phys. **2016**, *54*, 73–80

**KEYWORDS**: distributed Bragg reflectors; hyperbranched polymer; microcavity; multilayer; photonic crystals; polyvinylsulfides

**INTRODUCTION** In recent years, the development of photonic structures where periodical arrays of polymer films or building-blocks possessing different refractive index are assembled in highly ordered lattices with periodicity of the order of few hundreds of nanometers (Photonic Crystals, PhC) rose the academic and industrial interest.[1–5]

The advantages of using polymer PhC instead of more traditional inorganic materials rely on the opportunities provided in terms of low processing cost, large area, low weight, mechanical flexibility, and possibility to have free-standing structures suitable for postgrowth adhesion on preformed surfaces. This allows for the development of novel strategies for technological applications in the fields of bendable lasers,[6,7] sensors,[8,9] fabric,[10] and photovoltaic devices.[11,12]

By considering photonic crystal structures solely composed of polymer films, the main growth techniques usually adopted are based on block-copolymers self-assembly,[3,13,14] coextrusion,[15,16] and spin coating,[6,8,17–32] even though expensive and time consuming ones like holographic lithography,[33–36] or plasma vapor deposition (a technique suitable for radical polymerization only)[37,38] are also used. Among them, spin coating allows for a fast and simple preparation of one-dimensional (1D) planar PhC structures such as Distributed Bragg Reflectors (DBR, multilayers of two alternated materials) and microcavities (for an extended review on this topics, see ref. 39). In spite of clear advantages, several drawbacks limit the exploitation of such technique. Indeed, polymer materials suitable for that have to fulfil several constraints at once such as solvent orthogonality, compatible thermal properties (for post deposition thermal annealing), low light scattering (need for amorphous and/or controlled crystallinity polymers) and lack of electronic/vibrational transitions in the working spectral range. Moreover, they have to prevent solvent percolation and film swelling during growth and guarantee tight control of film thickness and interfacial roughness. All of them must be added to the main "optical" requirement for the structures: an as large as possible dielectric contrast, that is, a very large difference in refractive index ($\Delta n$) between the composing materials. The importance of this parameter is highlighted in Figure 1 where the calculated full width half maximum ($\Delta W$) of the photonic band gap (PBG) for a DBR is reported as a function of photon wavelength for polymer pairs having different $\Delta n$ (see

Additional Supporting Information may be found in the online version of this article.
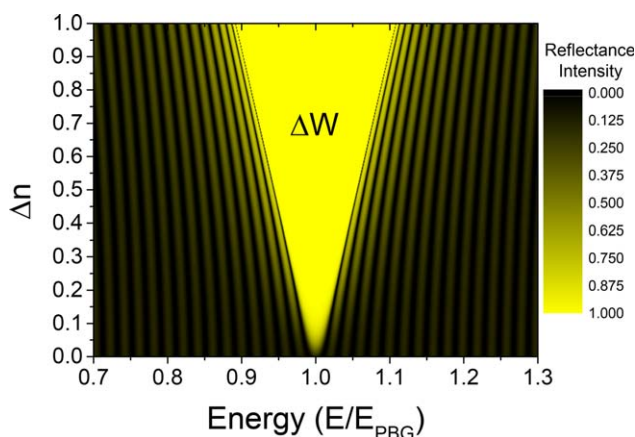
FIGURE 1 Color contour plot of the reflectance intensity spectra as a function of the dielectric contrast. The central yellow band highlights the PBG width ($\Delta W$). Notice: caption modified for black and white printing figures. [Color figure can be viewed in the online issue, which is available at wileyonlinelibrary.com.]

Table 1 for the refractive index of polymers commonly used for the preparation of such structures).

An analytical expression for $\Delta W$ is provided in the lambda fourth condition ($n_1 d_1 = n_2 d_2 = \frac{\lambda}{4}$; $D = d_1 + d_2$) according to eq 1

$$\frac{\Delta W}{E_{PBG}} = \frac{4}{\pi} \frac{|n_1 - n_2|}{n_1 + n_2} \qquad (1)$$

where $n_j$ and $d_j$ are the refractive index and thickness of the generic polymer $j$ and $D$ is the periodicity of the structure and $n_1 < n_2$.[1,40,41]

Currently, the most suitable polymer pair for PhC applications is CA:PVK, which provides a PBG width of about $5 \times 10^{-2}$,[42,43] while for a standard inorganic DBR SiO$_2$:TiO$_2$ ($\lambda = 1000$ nm:$n_{silica} = 1.46$, $n_{titania} = 2.48$)[44] $\Delta n = 1$ is achieved thus giving rise to $\Delta W > 0.2$. Notice that the dielectric contrast plays also a major role on the number of bilayers ($N$) needed to achieve high reflectance ($R$), according to eq 2:[1,40,41]

TABLE 1 Refractive Index (at $\lambda = 1000$ nm) of Polymers Often Used for the Growth of Planar Photonic Crystals Structures

| Polymer | $n^a$ | $\Delta n^b$ |
|---|---|---|
| Polytetrafluoroethylene (PTFE) | 1.33 | −0.13 |
| Poly(acrylic acid) (PAA) | 1.44 | −0.02 |
| Cellulose Acetate (CA) | 1.46 | 0 |
| Poly(vinyl alcohol) (PVA) | 1.53 | 0.07 |
| Poly(phenylene oxide) (PPO) | 1.57 | 0.11 |
| Polystyrene (PS) | 1.58 | 0.012 |
| PVK | 1.68 | 0.22 |

$^a$ See ref. 1 and references therein reported.
$^b$ With respect to CA, the low refractive index polymer mostly used for planar PhC structures growth.
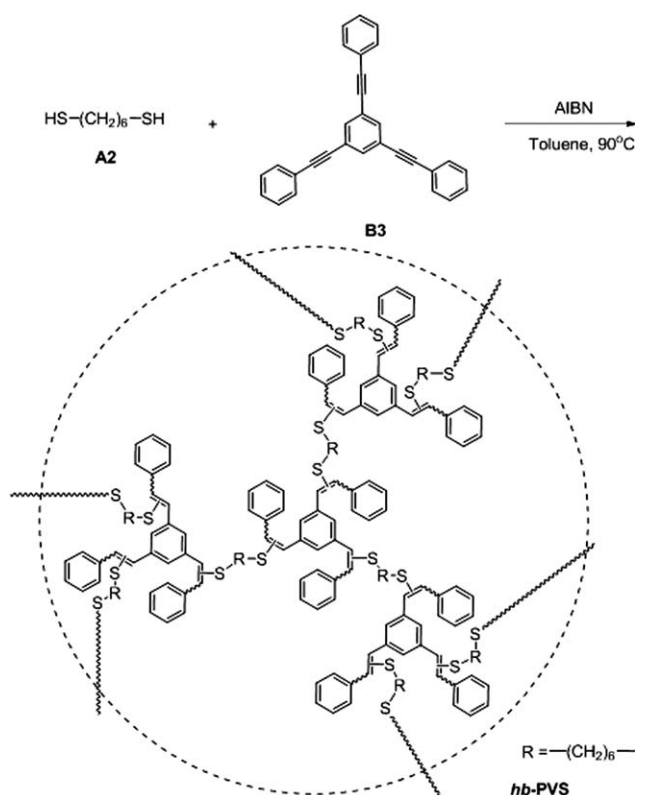


FIGURE 2 Scheme of the synthesis of HB polyvinylsulfide (HB-PVS).

$$R = 1 - 4 \left( \frac{n_1}{n_2} \right)^{2N}. \qquad (2)$$

In this way, high $\Delta n$ allows to achieve high reflectivity with a lower $N$, thus reducing problems that may be encountered during the growth process.[3,39] Finally, a larger $\Delta n$ allows to enhance all photonic properties in terms of spatial localization effects and light-matter interaction mechanisms.[24,40]

The search for high refractive index polymers is currently mainly focused on nanocomposites where metal-oxide nanocrystals are embedded into a polymer matrix.[45–47] In spite of the results achieved, they have never been tested for the fabrication of DBR where several constraints have to be fulfilled. Conjugated polymers are also known as high refractive index materials,[48–50] but they strongly absorb in the visible and are fluorescent. Consequently, they are more useful as photoactive materials than as transparent structural ones. It is also known that inverse vulcanized sulfur polymers possess very high refractive index,[51] but again they have not been tested yet for DBR production. However, the incorporation of sulfur atoms into a polymer skeleton containing conjugated moieties allows to obtain two increasing effects on the refractive index, thanks to the presence of heteroatoms (possessing a high electron density)[46,52] as well as to the pre-resonant condition for the near UV absorbing delocalized and highly polarizable $\pi$−electrons.[45] Indeed, linear and hyperbranched polyvinylsulfides (HB-PVS, Fig. 2), where sulfur incorporation and partial conjugation result from thiol–yne coupling with selective
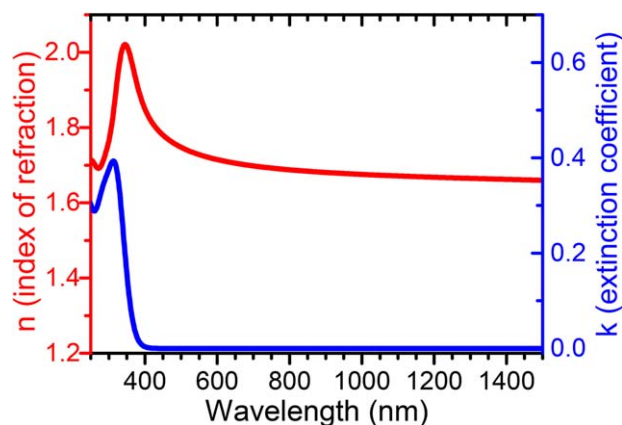
**FIGURE 3** Real (*n*) and imaginary (*k*) part of the complex refractive index of HB-PVS over a very broad spectral range. [Color figure can be viewed in the online issue, which is available at wileyonlinelibrary.com.]

mono-addition have been recently explored as high refractive index materials which might have use in antireflective coatings, displays, optical waveguides, organic lasers or light emitting diodes.[53–55] Especially the HB-PVS are of high interest in this regard due to their improved solubility and processability.

In this article, we report on the testing of HB-PVS for the fabrication of high optical quality DBR as well as photoactive materials in microcavities. A full spectroscopic characterization and theoretical modeling of the optical response of such structures is reported and discussed.

## EXPERIMENTAL

The HB-PVS used in this study was obtained through the reaction between 1,3,5-tribenzene-triethynebenzene ($B_3$) and the di-thiol $HS(CH2)_6SH$ ($A_2$) (Fig. 2). AIBN has been used as radical initiator and a monomer feed ratio of $A_2$:$B_3$=3:2 was applied. More details on the synthesis have been provided in ref. 53 The used HB-PVS was obtained after a reaction time of 20 h with $M_w = 41,600$ g/mol, $M_w/M_n = 17.3$ (RI detection, PS standard). HB-PVS is soluble in toluene (25–60 g/L) and then processable for DBR preparation when coupled with CA. Toluene solubility of HB-PVS was the crucial point for the success of the work since several solvents dissolve HB-PVS but a suitable orthogonality with diacetone-alcohol (the CA solvent) is achieved only with toluene. The polymer concentration in the solution affects the thickness of the layers and then allows to tune the PBG in different spectral ranges.[56] We would like to stress here that polymer concentration does not affect the number of bilayers needed to achieve a suitable reflectance intensity (see eq 2 and ref. 39).

DBR were fabricated alternating films of HB-PVS and CA ($M_W = 61,000$ g/mol). The polymer concentration ranged from 2.5 to 6% (w/v) and the rotation speed during the deposition was kept between 20 and 90 revolutions per second (rps); 100 $\mu$L of polymer solutions have been used for casting each layer. For microcavities growth, polyvinylcarbazole (PVK) toluene solutions with similar concentrations are also used.

DBR reflectance (R) and transmittance (T) spectra were collected using setups based on optical fibers coupled with Avantes 2048 spectrometers (200–1100 nm, resolution 1.4 nm) and with an Arcoptics FT-interferometer (900–2600 nm, resolution 8 cm$^{-1}$). The light source was a combined deuterium–halogen lamp model Micropak DH2000BAL. Collection angle resolved photoluminescence (PL) spectra are excited by a 405 nm CW laser (Oxxius S.A. LBX-405-100-CSB-PP model).[8,29] Steady state PL spectra of HBPVS have been also measured by using a Perkin Elmer MPF-44A spectrofluorimeter with excitation at 300 nm. PL intensities from excitation at different wavelengths were normalized at a constant value of the source intensity.

The optical response of DBR and microcavities has been calculated by an home-made code based on the Transfer Matrix Method[41] by using the polymer complex refractive index and layer thicknesses as input.

## RESULTS AND DISCUSSION

Figure 3 shows the complex refractive index ($n + ik$) of HB-PVS polymer over a very broad spectral range.

The imaginary part *k* (proportional to the absorption coefficient $4\pi k/\lambda$) is negligible up to 400 nm where the absorption onset is located then giving rise to a peak at 313 nm. In the transparent region, the refractive index is very high over all the investigated spectral range (about 1.68 at 1000 nm) and in the visible increases thus fostering the interest for HB-PVS. In the UV, where HB-PVS absorbs, n shows a peak at 345 nm.

Figure 4 shows the reflectance spectrum of a typical DBR prepared by alternating 10 bilayers of HB-PVS and CA as recorded on different positions of the sample (about one
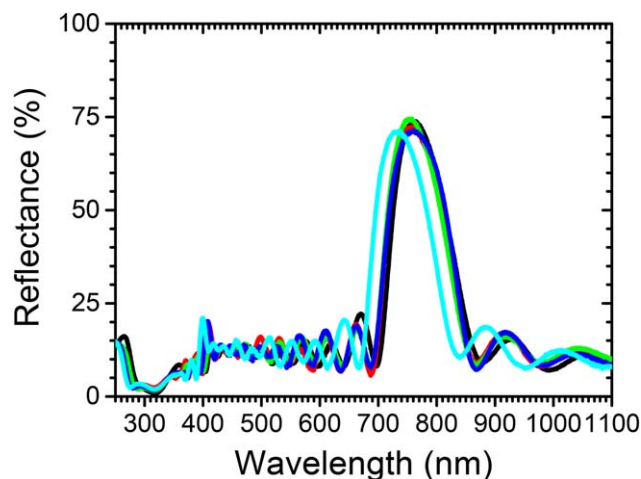


**FIGURE 4** Reflectance spectra for a 10 bilayers HB-PVS:CA DBR as recorded in different spots on the surface. The cyan spectrum corresponds to the center of the sample. Notice: caption modified for black and white printing figures. [Color figure can be viewed in the online issue, which is available at wileyonlinelibrary.com.]
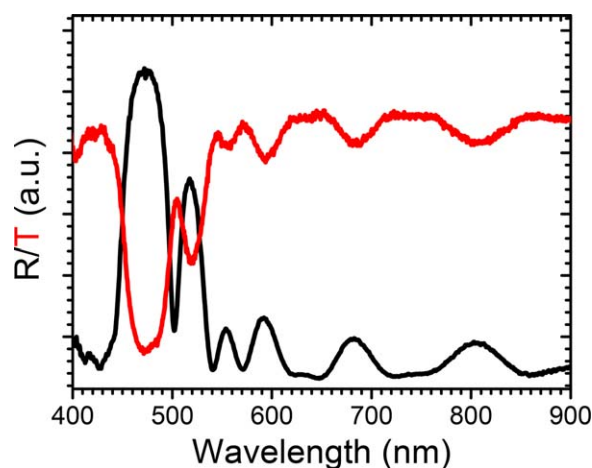
**FIGURE 5** Reflectance (black line) and Transmittance (red line) spectra of a HB-PVS microcavity sandwiched between two PVK:CA DBRs. Notice: caption modified for black and white printing figures. [Color figure can be viewed in the online issue, which is available at wileyonlinelibrary.com.]

inch side). A very strong reflectance peak is observed at $760 \pm 5$ nm depending on the recording spot. Only for the central part of the sample where the polymer solution is deployed, which is known to be typically the more disordered one, a larger spectral deviation is detected (734 nm). As a matter of fact, the interference fringes observed in the background of the spectra for the central position are different from those observed in the rest of the sample, indicating a different overall thickness of the multilayer.

The very good homogeneity combined with the very high reflectance intensity (measured above 70%, 76% calculated from eq 2) is indicative of the quality of the prepared DBR. For this kind of structures, the presence of second order diffraction peaks is also expected, being an even tighter fingerprint of optical quality.[6,8,24] In our samples, characterized by the principal PBG positioned around 760 nm, the second order is expected to be at $\lambda_{PBG}/2$–380 nm, which is however resonant with electronic transitions in HB-PVS, thus almost completely canceling it (except for a weak structure at 400 nm). Indeed, in the spectra of Figure 4, a very low signal is detected at such wavelengths and even interference fringes there disappear. This interpretation is confirmed by theoretical calculation of the optical response (Fig. SI1 of Supporting Information), reproducing the spectra by using the complex refractive index of HB-PVS reported in Figure 353 and CA[8] for film thicknesses $d_{HB-PVS} = 104$ nm and $d_{CA} = 142$ nm as input. The spectral tunability of the PBG can be obtained by changing the polymer concentration and/or the spinning velocity as shown in Supporting Information Fig. SI2.

To confirm the quality of the DBR structures so far produced, we investigated the dependence of their optical spectra as a function of the incidence angle (the photon momentum) both for polarization P and S (parallel and perpendicular to the plane of incidence, respectively, Supporting Information Fig. SI3). For

both polarizations, the PBG shifts toward higher energies upon increasing the incidence angle in a similar manner (Supporting Information Fig. SI3a, parallel; Fig. SI3b, perpendicular polarizations). For P-polarization, the PBG width decreases while for S-polarization it remains constant. Notice also that while for S-polarization the background of the spectra indicates a transmittance reduction, for P-polarization the behavior is less defined. This is in agreement with Fresnel equation for an effective medium, since for S-polarization the reflectance monotonically increases with the angle ($T = 1 - R$ decreases) while, for P-polarization the $R$ dependence on the incidence angle shows a minimum corresponding to the Brewster angle.[57] All properties of the spectra are in full agreement with theoretical modeling based on the transfer matrix method (Supporting Information Fig. SI3 c and d). Simple analytical expressions describing the angular dependence of the PBG can be provided in selected cases considering the effective refractive index and are briefly described in the Supporting Information.[41,58–60]

These results encouraged us to test HB-PVS as photoactive material embedded into a more sophisticated photonic structures. To this end, we prepared microcavities where a HB-PVS layer is sandwiched between two DBRs made of 10 bilayers PVK:CA. In this case, the PBG of the two DBRs sandwiching the cavity has been engineered around 500 nm, i.e. the spectral region where HB-PVS PL occurs (see below). As expected (Fig. 5), the line-shape of the PBG has been now modified by the cavity layer, acting both as structural defect breaking the translation symmetry of the multilayer and as refractive index dopant, since its refractive index is different than that of CA and PVK. The overall effect is the formation of a cavity mode, that is, the presence within the PBG of a sharp feature at about 505 nm (Fig. 5). Photons resonant with such cavity modes are allowed to propagate through the structure thus reducing the reflectance of the sample and increasing its transmittance. We would like to mention that the spatial uniformity of the microcavity is not as good as desirable. This indeed confirmed by the reflectance spectra recorded on different positions of its surface (see Fig. SI4 of Supporting Information). However, the main spectral fingerprint of the microcavity is still detected suggesting that further improvements in the processing could provide uniform samples over a large area.

Again, we investigated in more details the optical response of the microcavities. Figure 6 shows the microcavity transmittance spectra recorded as a function of the incidence angle for P- (a) and S-polarization (b). The PBG is observed as a yellow-green band around 500 nm for normal incidence. The cavity mode, which possesses a higher transmittance than the PBG, is the separation wall (bluish) between the yellow and green band. Both the cavity mode and the PBG shift toward lower wavelengths upon increasing the incidence angle. For P-polarization only, the PBG sharpens upon increasing the angle while for S-polarization the PBG $\Delta W$ is almost unchanged. These properties are similar to those previously described for the DBR (see also Supporting Information). The additional yellow/green bands in Figure 6 observed for photon energies far from the PBG are due
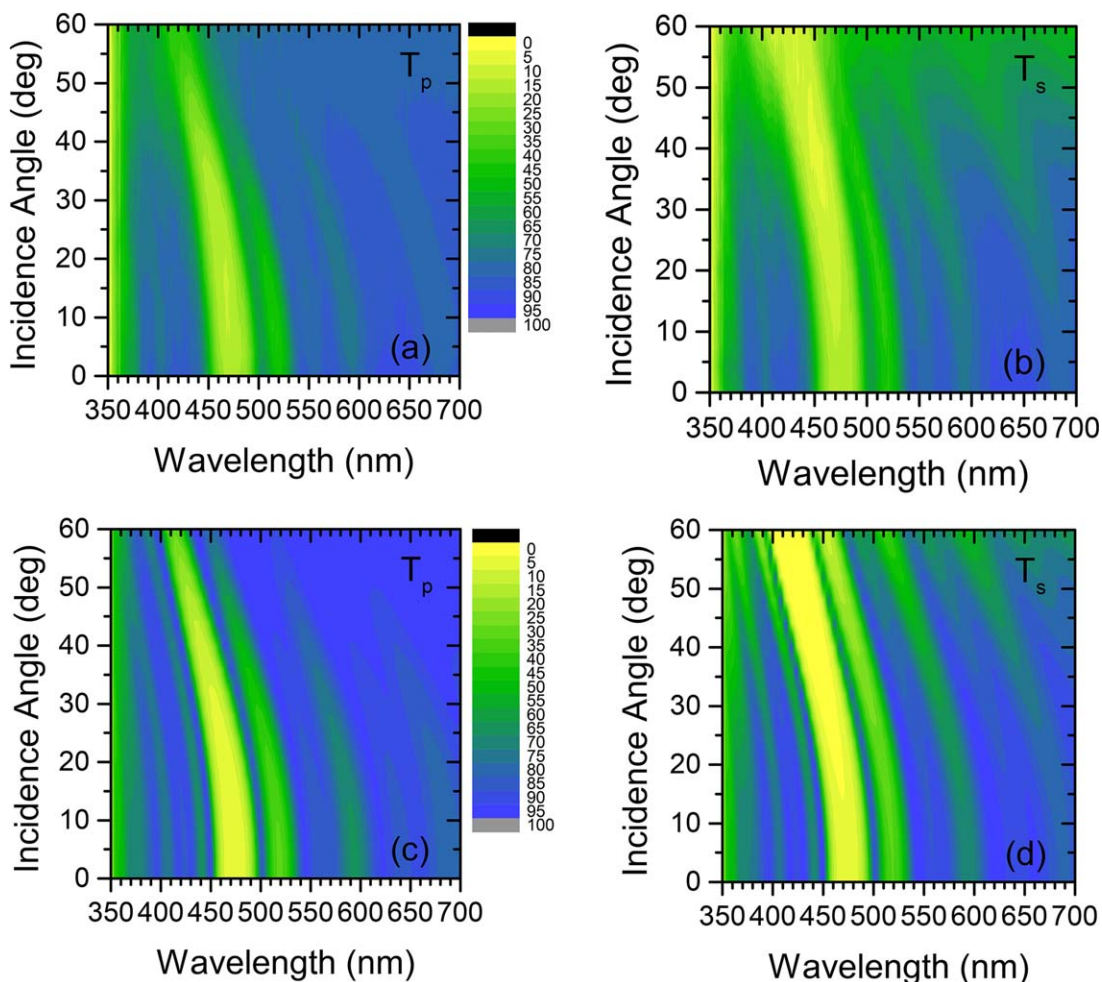
**FIGURE 6** Contour plots of transmittance spectra as a function of the incidence angle. (a,b) Experimental data; (c,d) theoretical data; Left panels, P-polarization; right panels, S-polarization. [Color figure can be viewed in the online issue, which is available at wileyonlinelibrary.com.]

to interference fringes, which modulate the background of the transmittance spectra. Their dispersion is due to the change on the probed sample thickness by changing the incidence angle.

All such properties can be finely reproduced by the theoretical spectra [Fig. 6(c,d)] calculated by using the refractive index of materials as input. The agreement between experiment and theory testifies once more the quality of the prepared photonic structures, and indirectly the good processability of HB-PVS.

As previously discussed, the microcavity has been engineered in order to be spectrally matched with the weak emission of HB-PVS (vide infra). By this way, we can test the fluorescence enhancement properties typical of such photonic structures. Indeed, it is well known that the defect layer of the microcavity allows for a strong localization of the electromagnetic field inside the cavity volume.[6,24,39] To demonstrate this, we have to compare the intensity of the fluorescence from the microcavity with a suitable standard for different detection angles. Notice that an absolute measurement by using an integrating sphere is unsuitable to this

end. Indeed, the directional emission from the PhC structures gets smeared out by the integrating sphere. However, suitable references for the comparison of the PL intensity have been demonstrated to be emitting material films cast in the very same conditions (substrate, solution concentration, spinning velocity, volume...), detuned microcavities as well as the same cavity after destruction of the PhC ordered structure.[24,61,62] The angle resolved PL for a reference HB-PVS film is reported in Figure 7 as dotted lines. HB-PVS broad spectra show a peak at about 485 nm and are almost independent on the detection angle. However, for the microcavity, severe changes are observed. At detection angle 0°, a new intense and sharp peak appears at 506 nm, almost corresponding to the cavity mode. It is assigned to two effects: the first one is a simple filtering effect due to the crossing of the PL light through the top DBR, which modulates the HB-PVS PL spectrum by the DBR transmittance one. This effect does not provide intensity enhancement.[61] The second one, much more important, is related to the cavity mode. Indeed, the microcavity modifies the density of photonic states (DOS) thus providing a more efficient interaction of the

electromagnetic field with the active layer and then giving rise to a redistribution of the fluorescence oscillator strength at different photon energies,[6,24] (see also Chapters 1, 4, 11, and 12 of ref. 1) where the DOS is peaked (see Fig. SI5 of Supporting Information).
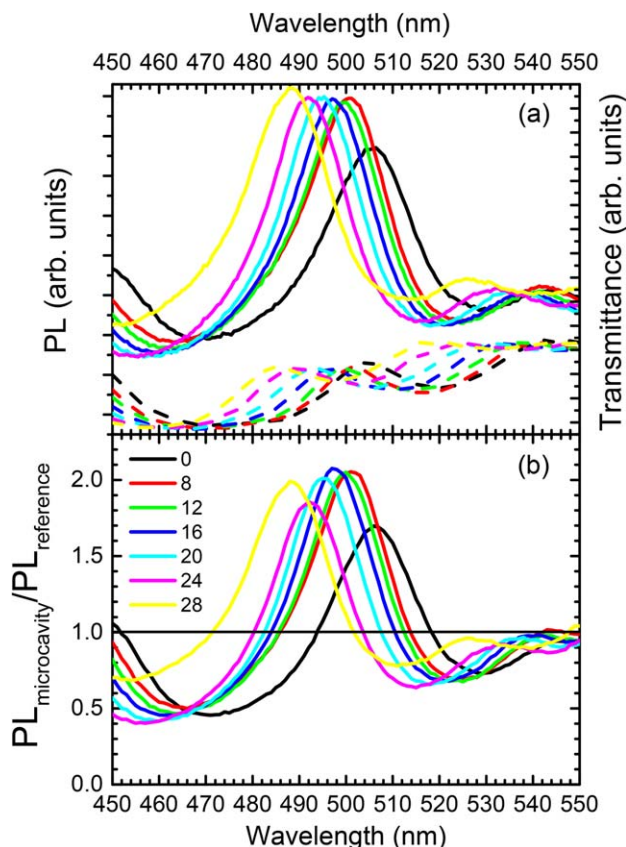
Upon changing the detection angle, the band at 506 nm shifts toward higher photon energies in agreement with the dispersion curves of the cavity mode observed in the transmittance spectra of the microcavity (Fig. 6).

This effect is highlighted in Figure 8 where the microcavity PL is directly compared to its transmittance spectrum recorded in the very same spot. We notice that for each angle, the sharp PL peak observed in the microcavity spectrum corresponds to the cavity mode in the transmittance one. This is a clear indication that such sharp emission observed in the microcavity PL spectrum is unambiguously due to the photonic structure. To better understand such items, it is useful to compare the PL and T spectra reported in Figure 8(a) with the fluorescence ratio spectra [Fig. 8(b)]. The PL ratio spectra are obtained dividing the PL spectra of the microcavity (as recorded at different angles) with the corresponding ones for the PL spectrum of the reference. The reference is used for two reasons. First, it allows to highlight the changes in the "spectral shape" of the microcavity with respect to those of the neat HB-PVS film. Second, it allows to evaluate the change in the "absolute intensity emission" of the microcavity. If the microcavity does not modify the emission with respect to the neat polymer film, the ratio spectrum should be equal to one.

PL photons within the band gap are not allowed to propagate. Indeed, the experimental data show a "reduction of PL" (PL ratio < 1) where the microcavity transmission spectra show the PBG fingerprint (about 450–490 nm and 520–
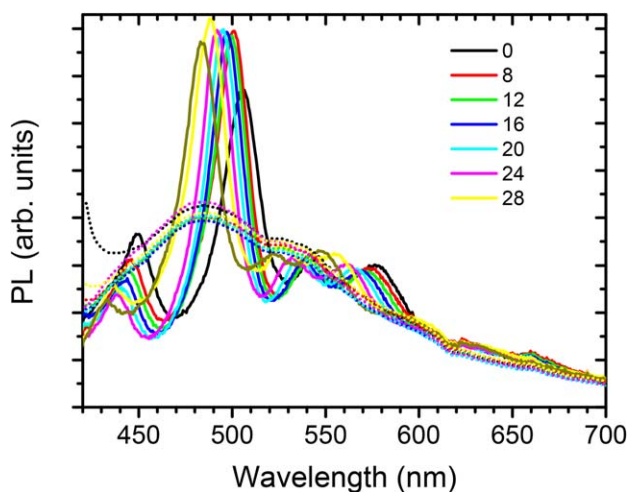


**FIGURE 8** (a) HB-PVS microcavity PL spectra (full line) as recorded at different collection angles compared with the corresponding transmittance spectra (dotted line). (b) Ratio between the PL spectra of the microcavity and those of the reference for the different detection angle. [Color figure can be viewed in the online issue, which is available at wileyonlinelibrary.com.]

550 nm at 0° detection). PL photons allowed to propagate through the cavity mode (about 490–520 nm at 0° detection) instead give rise to "ratio spectra larger than one." This means that the PL is enhanced with respect to the reference (PL ratio > 1). The reason for this behavior is related to the spectral shape of the DOS.[39] Photonic states in the gap are squeezed into the cavity mode thus providing a spectral redistribution of the PL spectrum and a corresponding increase of the PL signal. Outside the PBG spectral region, this effect does not exist since the structures behave like an effective medium. Indeed, outside the PBG region, the PL spectra of the microcavity and those of the reference are identical (see for instance Fig. 7 above 600 nm).

## CONCLUSIONS

We reported on the preparation of planar photonic crystal structures such as DBR and microcavities by using the high refractive index HB polyvinylsulfide HB-PVS. This polymer, never tested before to this end, allowed the preparation of DBR of high optical quality and good uniformity over an area of about of 1 inch squared. The same polymer has been also used as an active medium in microcavities. In spite of its



**FIGURE 7** Fluorescence spectra as a function of the detection angle for an HB-PVS film (dashed line) and the microcavity (full line) as detected from 0° to 28°, step by 4°. [Color figure can be viewed in the online issue, which is available at wileyonlinelibrary.com.]

weak fluorescence efficiency observed, HB-PVS microcavities showed fluorescence enhancement and spectral redistribution in full agreement to previous findings in the field. The optical response of all the prepared structures can be finely reproduced through optical modeling based on the transfer matric methods by using the complex refractive index of composing materials as an input. These results demonstrate that polyvinylsulfides are very good candidate as high refractive index materials for the preparation of all-polymer planar photonic crystal structures.

## ACKNOWLEDGMENTS

## REFERENCES AND NOTES

**1** D. Comoretto, Organic and Hybrid Photonic Crystals, 1 ed.; Springer International Publishing: Cham (CH), **2015**; p XXI, 497.

**2** L. D. Bonifacio, G. A. Ozin, A. C. Arsenault, *Small* **2011**, *7*, 3153–3157.

**3** J. H. Lee, C. Y. Koh, J. P. Singer, S. J. Jeon, M. Maldovan, O. Stein, E. L. Thomas, *Adv. Mater.* **2014**, *26*, 532–569.

**4** C. Liu, C. Yao, Y. Zhu, J. Ren, K. Lan, H. Peng, L. Ge, *RSC Adv.* **2014**, *4*, 27281–27285.

**5** Available at: http://opalux.com/. Accessed on June 19th, 2015.

**6** G. Canazza, F. Scotognella, G. Lanzani, S. D. Silvestri, M. Zavelani-Rossi, D. Comoretto, *Laser Phys. Lett.* **2014**, *11*, 035804

**7** L. M. Goldenberg, V. Lisinetskii, S. Schrader, *Appl. Phys. B* **2015**, 1–7.

**8** P. Lova, G. Manfredi, L. Boarino, A. Comite, M. Laus, M. Patrini, F. Marabelli, C. Soci, D. Comoretto, *ACS Photonics* **2015**, *2*, 537–543.

**9** J. E. Stumpel, C. Wouters, N. Herzer, J. Ziegler, D. J. Broer, C. W. M. Bastiaansen, A. P. H. J. Schenning, *Adv. Opt. Mater.* **2014**, *2*, 459–464.

**10** C. E. Finlayson, P. Spahn, D. R. Snoswell, G. Yates, A. Kontogeorgos, A. I. Haines, G. P. Hellmann, J. J. Baumberg, *Adv. Mater.* **2011**, *23*, 1540–1544.

**11** G. Lozano, S. Colodrero, O. Caulier, M. E. Calvo, H. Miguez, *J. Phys. Chem. C* **2010**, *114*, 3681–3687.

**12** A. Bozzola, V. Robbiano, K. Sparnacci, G. Aprile, L. Boarino, A. Proto, R. Fusco, M. Laus, D. Comoretto, L. C. Andreani, *Adv. Opt. Mater.* in press, doi:10.1002/adom.201500327.

**13** F. M. Hinterholzinger, A. Ranft, J. M. Feckl, B. Ruhle, T. Bein, B. V. Lotsch, *J. Mater. Chem.* **2012**, *22*, 10356–10362.

**14** C. Park, J. Yoon, E. L. Thomas, *Polymer* **2003**, *44*, 6725–6760.

**15** G. Mao, J. Andrews, M. Crescimanno, K. D. Singer, E. Baer, A. Hiltner, H. Song, B. Shakya. *Opt. Mater. Express* **2011**, *1*, 108–114.

**16** H. Song, K. Singer, J. Lott, Y. Wu, J. Zhou, J. Andrews, E. Baer, A. Hiltner, C. Weder, *J. Mater. Chem.* **2009**, *19*, 7520–7524.

**17** T. Komikado, S. Yoshida, S. Umegaki, *Appl. Phys. Lett.* **2006**, *89*, 061123.

**18** V. M. Menon, M. Luberto, N. V. Valappil, S. Chatterjee, *Opt. Express* **2008**, *16*, 19535–19540.

**19** L. M. Goldenberg, V. Lisinetskii, S. Schrader, *Laser Phys. Lett.* **2013**, *10*, 055808.

**20** L. M. Goldenberg, V. Lisinetskii, Y. Gritsai, J. Stumpe, S. Schrader, *Opt. Mater. Express* **2012**, *2*, 11–19.

**21** N. V. Valappil, M. Luberto, V. M. Menon, I. Zeylikovich, T. K. Gayen, J. Franco, B. B. Das, R. R. Alfano, *Photonic Nanostruct.* **2007**, *5*, 184–188.

**22** F. Scotognella, A. Monguzzi, M. Cucini, F. Meinardi, D. Comoretto, R. Tubino, *Int. J. Photoenergy* **2008**, *2008*, 389034

**23** S. Colodrero, A. Mihi, L. Häggman, M. Ocaña, G. Boschloo, A. Hagfeldt, H. Míguez, *Adv. Mater.* **2009**, *21*, 764–770.

**24** L. Frezza, M. Patrini, M. Liscidini, D. Comoretto, *J. Phys. Chem. C* **2011**, *115*, 19939–19946.

**25** L. Fornasari, F. Floris, M. Patrini, G. Canazza, G. Guizzetti, D. Comoretto, F. Marabelli, *Appl. Phys. Lett.* **2014**, *105*,

**26** A. L. Álvarez, J. Tito, M. B. Vaello, P. Velásquez, R. Mallavia, M. M. Sánchez-López, S. Fernández de Ávila, *Thin Solid Films* **2003**, *433*, 277–280.

**27** M. E. Calvo, S. Colodrero, N. Hidalgo, G. Lozano, C. Lopez-Lopez, O. Sanchez-Sobrado. H. Miguez, *Energy Environ. Sci.* **2011**, *4*, 4800–4812.

**28** S. Colodrero, M. Ocaña, A. R. González-Elipe, H. Míguez, *Langmuir* **2008**, *24*, 9135–9139.

**29** P. Lova, G. Manfredi, L. Boarino, M. Laus, G. Urbinati, T. Losco, F. Marabelli, V. Caratto, M. Ferretti, M. Castellano, C. Soci, D. Comoretto, *Phys. Stat. Solidi C* **2015**, *12*, 158–162.

**30** F. Scotognella, A. Monguzzi, F. Meinardi, R. Tubino, *Phys. Chem. Chem. Phys.* **2010**, *12*, 337–340.

**31** G. Qin, P. B. Dennis, Y. Zhang, X. Hu, J. E. Bressner, Z. Sun, W. J. Crookes-Goodson, R. R. Naik, F. G. Omenetto, D. L. Kaplan, *J. Polym. Sci. Part B: Polym. Phys.* **2013**, *51*, 254–264.

**32** J. Bailey, J. S. Sharp, *J. Polym. Sci. Part B: Polym. Phys.* **2011**, *49*, 732–739.

**33** E. Pialat, T. Trigaud, J. P. Moliton, M. Thévenot, *J. Polym. Sci. Part B: Polym. Phys.* **2007**, *45*, 2993–3002.

**34** W. Lee, S. A. Pruzinsky, P. V. Braun, *Adv. Mater.* **2002**, *14*, 271.

**35** Y. Zhong, L. Wu, H. Su, K. S. Wong, H. Wang, *Opt. Express* **2006**, *14*, 6837–6843.

**36** L. Wu, Y. Xu, K. S. Wong, In Organic and Hybrid Photonic Crystals; D. Comoretto, Ed.; Springer, **2015**; Chapter 10.

**37** A. Convertino, A. Valentini, R. Cingolani, *Appl. Phys. Lett.* **1999**, *75*, 322–324.

**38** A. Coclite, In Organic and Hybrid Photonic Crystals; D. Comoretto, Ed.; Springer International Publishing: Cham (CH), **2015**; p 167–186.

**39** F. Scotognella, S. Varo, L. Criante, S. Gazzo, G. Manfredi, R. Knarr, D. In Organic and Hybrid Photonic Crystals; D. Comoretto, Ed.; Springer: Cham (CH), **2015**; p 77–101.

**40** J. D. Joannopoulos, R. D. Meade, J. N. Win, Photonic Crystals: Molding the Flow of the Light Princeton University Press: Princeton (USA), **1995**.

**41** M. Skorobogatiy, J. Yang, Fundamentals of Photonic Crystal Guiding; Cambridge University Press: Cambridge (UK), **2009**.

**42** Fluorinated polymers are known to possess very low refractive index ($n = 1.33$) but their processability is very difficult from solutions. As far as we know, few attempts have been reported on the use of fluorinated polymers for the preparation of DBR by plasma vapor deposition (see for instance refs. 37 and 38) or by coextrusion (ref. 16). Such techniques cannot be used with all polymers (in particular the functional ones) thus limiting their use. Some of the authors of the manuscript are working on the deposition of fluorinated polymers from solutions in order to obtain photonic structures but such results cannot be disclosed since a patent request is pending.

**43** Poly(acrylic acid) is instead been successfully used for the preparation of DBR (ref. 21). However, nobody reported the details of the polymer used. Since some of the forms available on the market is cancerogenic, this material is less commonly used to prepare DBR structures. From Sigma-Aldrich web site http://www.sigmaaldrich.com/catalog/search?term=poly+acrylic+acid&interface=All&N=0&mode=match%20partialmax&lang=it&region=IT&focus=product (access date August 17, 2015), for Poly(acrylic acid) CAS Number 9003-01-4 products Mw=N.A. (323667), Mn=130000 typical (181293), Mv ~1,250,000 (306215), the Material Safety Data Sheets (MSDS) do not report specific safety problems unless the sentence "this product is or contains a component that is not classifiable as to its carcinogenicity based on IARC, ACGIH, NTP, or EPA classification". On the other hand, for products Mv ~450,000 (181285) and Mv ~3,000,000 (306223), MSDS reports "TOXIC R45 and R46, MUTAGENIC H340, CANCEROGENIC H350.

**44** M. Polyanskiy, RefractiveIndex.INFO. Available at: http://refractiveindex.info/, Accessed June 19, 2015.

**45** J. Liu, M. Ueda, *J. Mater. Chem.* **2009**, *19*, 8907–8919.

**46** C. Lu, B. Yang, *J. Mater. Chem.* **2009**, *19*, 2884–2901.

**47** M. Russo, M. Campoy-Quiles, P. Lacharmoise, T. A. M. Ferenczi, M. Garriga, W. R. Caseri, N. Stingelin, *J. Polym. Sci. Part B: Polym. Phys.* **2012**, *50*, 65–74.

**48** C. Soci, D. Comoretto, F. Marabelli, D. Moses, *Phys. Rev. B.* **2007**, *75*, 075204

**49** D. Comoretto, G. Dellepiane, F. Marabelli, J. Cornil, D. A. dos Santos, J. L. Bredas, D. Moses, *Phys. Rev. B* **2000**, *62*, 10173–10184.

**50** C. M. Ramsdale, N. C. Greenham, *Adv. Mater.* **2002**, *14*, 212–215.

**51** J. J. Griebel, S. Namnabat, E. T. Kim, R. Himmelhuber, D. H. Moronta, W. J. Chung, A. G. Simmonds, K. J. Kim, J. van der Laan, N. A. Nguyen, E. L. Dereniak, M. E. Mackay, K. Char, R. S. Glass, R. A. Norwood, J. Pyun, *Adv. Mater.* **2014**, *26*, 3014–3018.

**52** D. W. v. Krevelen, K. T. Nijenhuis, Properties of Polymers; Elsevier B.V., Amsterdam (The Netherlands), **2009**; Chapter 10.

**53** R. Pötzsch, B. C. Stahl, H. Komber, C. J. Hawker, B. I. Voit, *Polym. Chem.* **2014**, *5*, 2911–2921.

**54** Q. Wei, R. Pötzsch, H. Komber, D. Pospiech, B. Voit, *Polymer* **2014**, *55*, 5600–5607.

**55** R. Pötzsch, H. Komber, B. C. Stahl, C. J. Hawker, B. I. Voit, *Macromol. Rapid Commun.* **2013**, *34*, 1772–1778.

**56** D. B. Hall, P. Underhill, J. M. Torkelson, *Polym. Eng. Sci.* **1998**, *38*, 2039–2045.

**57** E. Hecht, Optics; Addison-Wesley: San Francisco (USA), **2002**.

**58** D. Antonioli, S. Deregibus, G. Panzarasa, K. Sparnacci, M. Laus, L. Berti, L. Frezza, M. Gambini, L. Boarino, E. Enrico, D. Comoretto, *Polym. Int.* **2012**, *61*, 1294–1301.

**59** R. J. Gehr, R. W. Boyd, *Chem. Mater.* **1996**, *8*, 1807–1819.

**60** D. Bajoni, Optical Spectroscopy of Photonic Crystals and Microcavities; University of Pavia: Pavia, **2004**.

**61** L. Berti, M. Cucini, F. Di Stasio, D. Comoretto, M. Galli, F. Marabelli, N. Manfredi, C. Marinzi, A. Abbotto, *J. Phys. Chem. C.* **2010**, *114*, 2403–2413.

**62** F. Di Stasio, L. Berti, S. O. McDonnell, V. Robbiano, H. L. Anderson, D. Comoretto, F. Cacialli, *APL Mater.* **2013**, *1*, 9.